Hindawi
International Journal of Antennas and Propagation
Volume 2023, Article ID 6457969, 17 pages
https://doi.org/10.1155/2023/6457969

Research Article

Novel Meandered Line EBG Filters with Significant Size Reduction Using Sine Tapering

S. M. Shakil Hassan, [1,2] **Kalyan Kumar Halder**, [1] **and Md. Nurunnabi Mollah** [1]

[1] *Department of Electrical and Electronic Engineering, Khulna University of Engineering & Technology, Khulna, Bangladesh*
[2] *Department of Electrical and Electronic Engineering, Eastern University, Dhaka, Bangladesh*

Correspondence should be addressed to S. M. Shakil Hassan; shakil.bq@gmail.com

Received 3 May 2023; Revised 3 August 2023; Accepted 25 August 2023; Published 4 October 2023

Academic Editor: Ashish Gupta

Tapering electromagnetic bandgap (EBG) structures is a common method in designing microstrip filters with different periodic structures. A novel technique for tapering EBG structures with the amplitude coefficients obtained from the sine function has been illustrated. This method deduces mellifluous coefficients that improves the performance with reasonable stopband width, preferable insertion loss level, and much-minimized passband ripples compared to similar designs with other tapering methods (e.g., binomial distribution, Chebyshev distribution, and conventional cosine tapering). It also offers tandem use of tapered EBG structures, leading to the novel meandered transmission line tandem design that significantly reduces the length of the filter; more than 40% is possible, compared to the uniform and conventional tapered designs. Size reduction on such a large scale will benefit the designers with the limited space issues.

1. Introduction

Planer electromagnetic bandgap (EBG) structures are periodic elements in the ground plane of a microstrip transmission line. They have found much attraction for exhibiting bandpass and band rejection properties at microwave and millimeter wave frequencies. Because of their unique property of impeding surface waves, EBG structures have found potential applications in planner transmission lines for realizing different types of microwave filters, phased array antennas, waveguides, high-efficiency power amplifiers, diplexers, power dividers/combiners, and many other devices [1–5]. EBG structures are of different shapes, for example, circular, square, annular ring, spiral, triangular, and dumbbell-shape [5–11]. In much earlier literature, EBG structures were termed photonic bandgap (PBG) structures [7]. However, several techniques for improving the performance of EBG-assisted filters and antennas have been investigated; one of the popular methods for optimum filter design is tapering the EBG elements [12–14].

Tapering of EBG structures has become a very popular trend in designing EBG-assisted microstrip transmission lines due to its significant impact on improving performance in terms of lower ripple heights (RHs) at passband frequencies [15–17]. Tapered EBG structures are also called nonuniform EBG structures [7]. They possess a lower total etching area (A_{TE}) compared to the respective uniform EBG structures-assisted microstrip transmission line; therefore, the maximum level of the insertion loss (IL or the S_{21} curve of the S-parameter performance) becomes lower. However, several techniques for creating nonuniform EBG structures have been reported in the open literature: these include binomial, Blackman, Chebyshev, Gaussian, Hamming, Welch, and others [18–20]. Among them, the Chebyshev distribution has found a wide range of applications for offering the most promising performance, but it requires substantial effort to solve large equations to get the desired tapering coefficients [21–23].

All of the tapering functions have several inadequacies with the single advantage of offering a much smaller ripple in the passband. The challenges are as follows:

(1) They reduce the stopband width (SBW) significantly as the sizes of the EBG patterns reduce dramatically.
(2) The IL level becomes much lower due to having an inadequately distributed total etching area.
(3) The size of the reference EBG element must be extremely large to provide a sufficient, evenly distributed etching area.
(4) To get appreciable performance, amplitude coefficients have to be selected for too many EBG elements.
(5) Thus, the total number of EBG structures increases; hence, the length of the transmission line becomes unnecessarily longer [18].
(6) EBG patterns at both ends become too small to have significant impacts on performance [24].

In this paper, we have demonstrated a simpler technique of finding the tapering coefficients using the sine function. We have demonstrated the tapering coefficient factor (T_{cf}) as a means to evaluate different tapering functions. We have shown that tapering of EBG patterns by the area of the reference EBG element instead of its size (e.g., the radius of a circular or the side of a square EBG structure) is more beneficial.

Furthermore, the sine tapering method mathematically and systematically supports the tandem use of tapered EBG structures that yields the tandem design; based on the tandem design, we have introduced a novel meandered transmission line lattice of EBG structures with reduced physical size of the filter realizations.

2. Design Procedure of EBG Filters

In Figure 1, we can see the basic designs of a uniform EBG structure-assisted microstrip transmission line, where the transmission line is at the top plane and EBG patterns are at the ground plane; these designs are supposed to behave as a bandstop or notch filter. We can see that the inner structure or inner element spacing (i.e., period) is denoted as "a" as follows:

$$a = \frac{\pi}{\beta}, \tag{1}$$

where β is the wavenumber in the dielectric slab, which can be expressed as follows:

$$\beta = \frac{2\pi f_0}{c}\sqrt{\varepsilon_e}, \tag{2}$$

where f_0 is the considered center frequency of the stopband, ε_e is the effective relative permittivity of the used dielectric substance, and c is the speed of light in free space.

Besides in Figure 1, we can see that the number of periodic EBG structures is denoted as "n": for example, $n = 7$ and 6 are shown in Figures 1(a) and 1(b) for uniform circular and square EBG structures, respectively. The size of the EBG element can be determined using the filling factor (FF) as defined by the following generalized expression [6]:

$$\mathrm{FF} = \frac{\text{area of an EBG element } (\mathrm{A}_{\mathrm{EBG}})}{\text{area of a unit cell } (\mathrm{A}_{\mathrm{cell}})}. \tag{3}$$

Tapering is done with a set of coefficients known as amplitude or tapering coefficients (k), where the sizes of the adjacent EBG elements are proportional to the size of the reference EBG element with the corresponding k; two typical tapered designs are shown in Figure 2 for both odd and even values of n. A more detailed process of such a tapered design is discussed in later sections.

However, in our study, we have used Taconic substrate, which has relative permittivity (ε_r) and thickness (h) of the substrate as 2.45 and 31 mils, respectively. Hence, the width (w) of the standard $50\,\Omega$ transmission line is 2.264 mm. We have considered $f_o = 10$ GHz, and thus $a = 10.5$ mm. These parameters are kept identical for all the designs that we have realized for investigation, unless specified otherwise.

3. Different Filters Design, Simulations, and Measurements

In this paper, we have used a method of moments-based software from Mentor Graphics (formerly Zeland Software, Inc.) named IE3D, a widely used software, and experts have found that the simulated results agree well with the measured results [22, 23]. We have investigated the merits of the congruency of our simulations using this software by comparing the simulated performances of some earlier reported designs with measured performances too.

3.1. Uniform EBG Design. A nontapered nine circular EBG elements-assisted design is realized on the substrate having a dielectric constant of $\varepsilon_r = 10.2$ and a thickness of $h = 1.27$ mm. The width of the transmission line is $w = 1.2$ mm, the radius is $r = 3.525$ mm, and inner element spacing is $a = 14.1$ mm [18]. We have simulated the same EBG filter and compared the simulated S-parameter performance with the reported measured performance, as shown in Figure 3(a). The measured result shows slightly larger passband ripples, a little larger stopband, and a higher rejection level than the simulated result. Such minor dissimilarities are insignificant and are very common in experimental results because of the limitations of measurement tools and since very precise etching of EBG elements is hardly possible in practice.

3.2. Cosine-Tapered EBG Design. By determining the cosine-tapering coefficients using (6), we have designed and simulated the cosine-tapered design as reported in [18]. The radius of the reference circular EBG pattern $r_{\mathrm{ref}} = 3.525$ mm. A comparison of the reported measured result and the simulated results using IE3D is shown in Figure 3(b). Although the insertion loss curve of the measured and simulated results follows a similar fashion, the SBW and the maximum IL level are a bit higher in the measured result as observed in the abovementioned design.

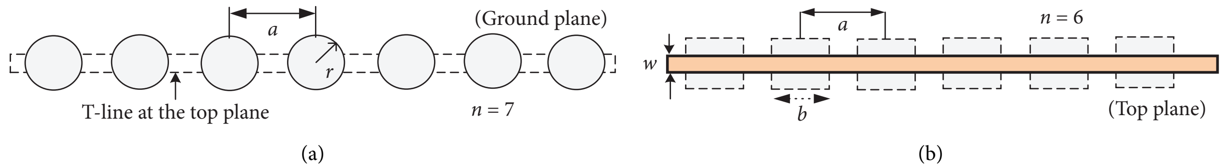

Figure 1: Uniform EBG structure-assisted microstrip bandstop filters with (a) circular and (b) square EBG patterns at the ground plane.

3.3. Chebyshev-Tapered EBG Design. For further verification, we have designed and simulated a Chebyshev-tapered design reported in [25]. The comparison of the simulated and the measured result is shown in Figure 4, where we can see that except for a very little deviation, the simulated results agree very well with the measured results.

In the above-investigated designs, we have found very minor dissimilarities, and those are well accepted by researchers around the world. Therefore, we have found enough confidence to simulate and analyze the other designs using the IE3D software. We are highly convinced that all the simulated results will agree well with the measured results.

4. Sine Tapering vs. Reported Cosine, Chebyshev, and Binomial Tapering Function

In this section, we have discussed the proposed method of sine tapering and the traditional cosine tapering that are reported in open literature: [18, 23].

4.1. Fundamentals of Sine Tapering Function. The tapering coefficients of a sine function for the preferred n have to be calculated as follows:

$$k_i = |\sin(i \times \Delta\theta)| = \left|\sin\left(\frac{\pi i}{n+1}\right)\right|, \quad (4)$$

where $i = 1, 2, 3, \ldots, n$ denote the positions of the EBG element and $\Delta\theta$ is the angular spacing of each EBG element between 0° and 180° or (0 to π radians) of the sine function to get coefficients for n EBG elements. For instance, if $n = 5$ and 6, then $\Delta\theta$ is 30° and 25.71°, respectively.

Now, the size of the EBG elements can be calculated by multiplying the tapering coefficients with the size of the reference EBG element as follows:

$$x_i = k_i \times x_{\mathrm{ref}}, \quad (5)$$

where x_{ref} is the dimension of the reference EBG element; x, for example, can be radius (r) or arm length (b) for circular or square EBG patterns, respectively [24]. x_i is the size of the i^{th} EBG element. Nonuniform or tapered designs having odd and even numbers of EBG patterns are shown in Figure 2.

4.2. Fundamentals of Cosine Tapering Function. A detailed method of finding the coefficients using the cosine tapering function is depicted by Huang and Lee as follows:

$$k_i = \cos\left(\frac{\pi}{2} \times z_i\right), \quad (6)$$

where z_i is the normalized distance of the i^{th} EBG element from the center of the transmission line [23], and it is defined as follows:

$$z_i = \frac{2d_i}{L_t}, \quad (7)$$

where d_i is the actual distance of the i^{th} EBG element from the center of the transmission line and L_t is the actual minimum length of the transmission line. L_t is determined by

$$L_t = (n-1)a + x_0, \quad (8)$$

where x_o denotes the dimension of the fundamental or reference EBG structure; for example, x_o represents the diameter (D_o) for a circular EBG structure or the side length (b_o) for a square EBG structure.

Besides, Laso et al. defined the cosine tapering function as follows:

$$k_i = T\left(\frac{z}{L}\right) = \left(\cos\left(\pi\frac{Z}{L}\right)\right)^{0.5}, \quad (9)$$

where z/L is the normalized longitudinal position [18].

Thus, coefficients determined by using (6) and (9) are not identical; besides, both equations depend on the period, the number of EBG elements, and the shape and size of the EBG pattern.

From (6), the length of the actual minimum of the transmission line depends on the size, shape, and period (a) of the EBG patterns and, like other tapering methods, obviously on the number of EBG elements (n). Therefore, for a given number of EBG structures, the cosine-tapering coefficients depend on the period, a, and the size and the shape of the EBG structures, whereas k_i of the sine tapering is independent of such variables, but only n.

4.3. Chebyshev and Binomial Tapering Functions. Chebyshev coefficients are related to the Dolph–Tschebyscheff array and polynomial, where designers need to go through a relatively complicated and longer process of calculations to determine the tapering coefficients for different numbers of EBG elements [21–23]. In contrast, the sine tapering coefficients are much easier to determine.

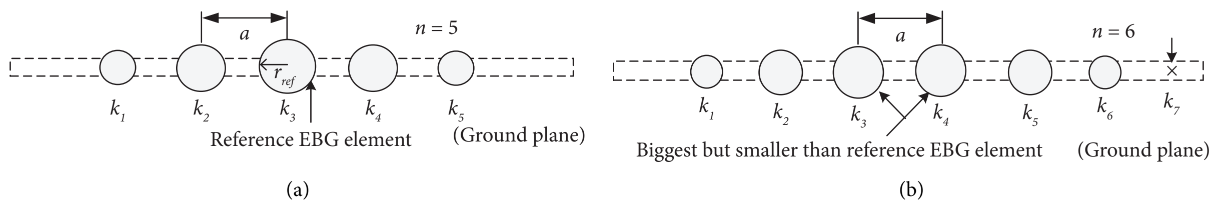

Figure 2: Tapered circular EBG structures using sine function, where (a) n is odd (i.e., 5) and (b) n is even (i.e., 6).

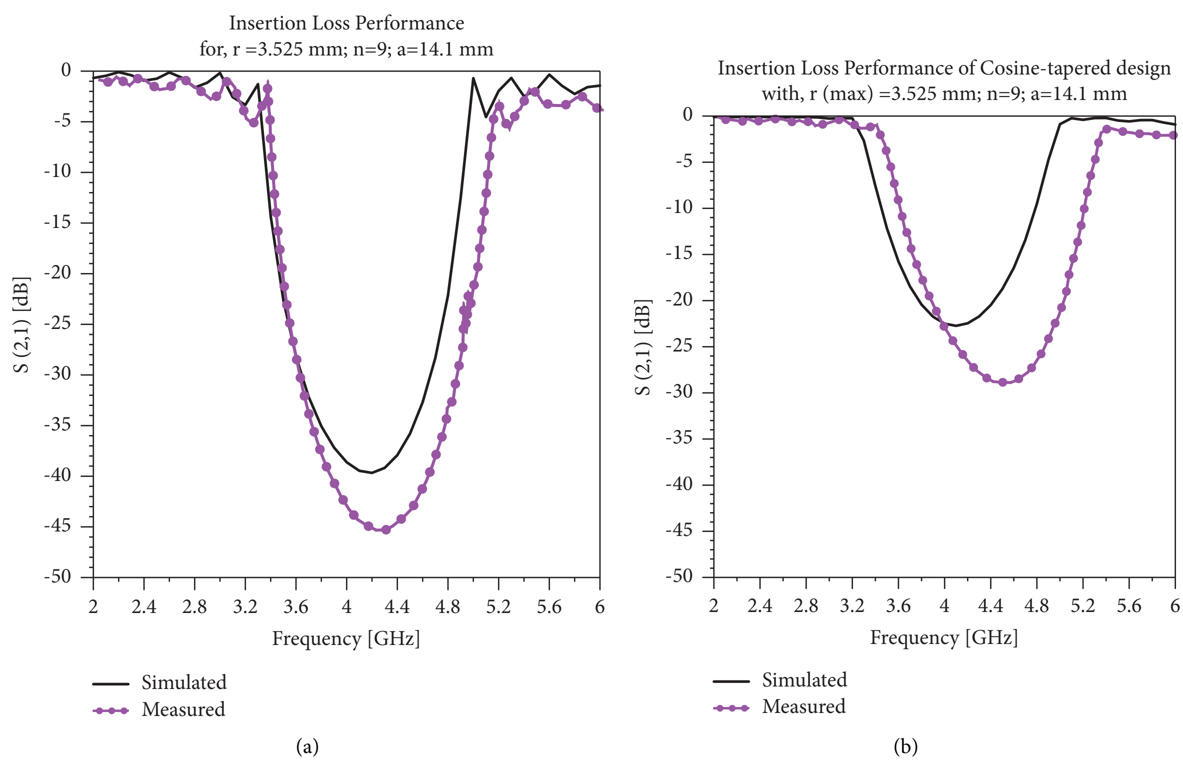

Figure 3: Reported measured result in [18] vs. simulated insertion loss parameters of (a) uniform nine circular EBG elements-assisted design and (b) cosine-tapered design. Substrate: $\varepsilon_r = 10.2$ and $h = 1.27$ mm.

On the other hand, binomial coefficients can easily be determined using Pascal's triangle derived from binomial polynomials [21, 23, 26].

4.4. Merit of the Tapering Functions. Tables 1 and 2 show the differences in different tapering coefficients for different shapes, sizes, and periods. From the table, we can see that the tapering coefficient factor expresses the merit of tapering different tapering functions for a given n.

T_{cf} is defined as follows:

$$T_{\mathrm{cf}} = \frac{\sum_{i=1}^{n} k_i}{n}, \tag{10}$$

where $T_{cf} = 1$ means the uniform design and $T_{cf} = 0$ means a blanked transmission line or simple microstrip line.

We can observe from Table 1 that the values of the coefficients for the cosine function for circular and square EBG patterns are different, and so is T_{cf}, besides, for different inner element spacing, they get changed too. In Table 2, the coefficients of the sine and cosine tapering functions are compared for different numbers of EBG structures. We have observed that the cosine function results in a much smaller T_{cf} than the sine function; whereas T_{cf} of Chebyshev and sine-tapering functions are very close.

5. Performance of Sine-Tapered Designs in Comparison to Other Designs

In this section, we will investigate the performance of sine-tapered designs, and the performances will be compared with the uniform design and with binomial, Chebyshev, and cosine-tapered designs. Besides, we will accomplish the comparison in two different tapering categories, namely, "*size tapering*" and "*area tapering*."

We have considered the following parameters for designing the EBG filters for our investigations: $\varepsilon_r = 2.45$; $h = 31$ mils; $w = 2.264$ mm; $f_o = 10$ GHz; and $a = 10.5$ mm.

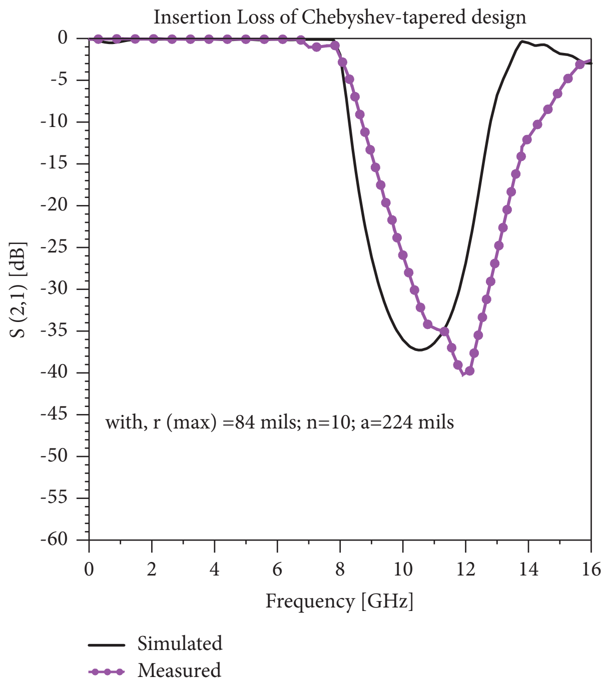

FIGURE 4: Reported measured result in [25] vs. simulated insertion loss parameter of the Chebyshev-tapered design. Substrate: $\varepsilon_r = 10.2$ and $h = 25$ mils.

5.1. Uniform Design. To evaluate the merit of the sine tapering function by performing a comparative analysis on the performance of different tapering functions, we have considered two design variables: the size of the reference EBG element, as uniform designs, and the number of the EBG elements.

Performances of the uniform square shape EBG element-assisted designs for two different sizes and different numbers of elements are tabulated in Table 3; we observe that as the size and the number of EBG elements increase, the IL increases and results in a wider −20 dB rejection bandwidth [25, 27].

The uniform designs usually suffer from spurious ripples in the passband and thus result in poor RL performance. Figure 5(a) shows the scattering parameters of a uniform design, with $n = 6$ and $b_{\text{ref}} = 6.2$ mm, that results in −20 dB rejection bandwidth (BW) of 5.885 GHz and a maximum level of isolation (S_{21}) of −50.57 dB; but at the center frequency, 10.416 GHz, the isolation is −48.98 dB. Moreover, the −10 dB RL bandwidth which is also known as passband width (PBW) is 6.151 GHz. Here, −5.19 dB maximum passband ripple and 7.036 GHz −3 dB cutoff frequency are observed. As can be seen in Table 3, uniform designs exhibit poor RL performance near the cutoff frequency, with high spurious ripple on S_{21} in the passband (in Figure 5). These ripples can be significantly minimized by using tapering methods that, in effect, improve complete performance.

5.2. Size Tapering. The tapering coefficients are applied directly to the dimension-denoting parameters of EBG structures that yield size tapering. In Figure 5 and Table 3, we see that for the binomial function, since the values of the tapering coefficient are too small (i.e., T_{cf} is lower, see Tables 1 and 2), the IL performance is very poor. On the other hand, the Chebyshev and sine tapering functions have a higher T_{cf} and exhibit very impressive S-parameter performance in terms of IL and RL performance. However, the cosine function results in moderate performance, much better than the binomial tapering, but the performance is not much attractive compared to Chebyshev-tapering methods.

Besides, the novel sine tapering method exhibits a little better performance than the Chebyshev method (Figure 5); therefore, the best performance is observed from the sine tapering method. In general, all the tapering functions improve the overall performance by reducing the passband RHs, but at the expense of the SBW. As seen from Table 3 and Figure 5, size tapering results in much smaller sizes of EBG structures; hence, the performances of these designs are too deviated and poor compared to the respective uniform designs. In the table for the design, with $n = 6$ and $b_{\text{ref}} = 6.2$ mm, we can see that SBW for the uniform design is 5.885 GHz, but for the binomial tapering, no appreciable stopband is formed. SBWs for the cosine, Chebyshev, and sine tapering are 2.484 GHz, 3.751 GHz, and 4.063 GHz, respectively, and the maximum passband RHs are much lower for all. From the whole study, we can observe that among the compared tapering functions, the novel sine tapering method shows better performance.

5.3. Area Tapering. We have observed that different shapes of conventional EBG structures perform identically, having identical etching areas [6]. Therefore, instead of the size, we prefer the area of conventional EBG structures for analyzing their performances. Thus, we rewrite (5) in terms of the area of the EBG elements as follows:

$$A_i = k_i \times A_{\text{ref}}, \tag{11}$$

where A_{ref} is the area of the reference EBG element and A_i is the area of the i^{th} EBG element after tapering.

Figure 5(c) shows the performances of the tapered designs, where area tapering is realized for the same reference EBG element as for the size tapering analysis; the performances are tabulated in Table 4. By comparing Figures 5(a) and 5(c), we can easily observe that the area tapering method shows better performance than the size tapering method for all the tapering functions; since SBW and the maximum level of isolation get increased with a very small increment in RH, passband ripples are still considered to be within an acceptable range. As in Table 4, for the design with a square EBG pattern of the side length of 6.2 mm and with $n = 10$, the maximum RH observed is −1.00 dB, and the SBW is 5.482 GHz (wider than other); the SBW is almost 90% of the uniform design, and the RH is 72% lower than the non-tapered or uniform design.

Now, when we compare the performances of tapered designs to T_{cf} shown in Tables 1 and 2, we can see from Tables 3 and 4 that with higher T_{cf} (except $T_{cf} = 1$, uniform design), the performance of S_{21} improves noticeably. The sine tapering function offers relatively higher values of

Table 1: Tapering coefficients obtained from different methods for $n = 6$.

Tapering function	a (mm)	Shape; size (mm)	k_1	k_2	k_3	k_4	k_5	k_6	T_{cf}
Binomial			0.1	0.5	1.0	1.0	0.5	0.1	0.533
Chebyshev	×	×	0.39	0.73	1.0	1.0	0.73	0.39	0.707
Sine			0.43	0.78	0.97	0.97	0.78	0.43	0.727
Cosine	10.5	Circular; $r_0 = 3.5$	0.18	0.67	0.96	0.96	0.67	0.18	0.603
		Square; $b_0 = 6.2$	0.17	0.67	0.96	0.96	0.67	0.17	0.600
	15	Square; $b_0 = 4.7$	0.09	0.63	0.96	0.96	0.63	0.09	0.560
		Square; $b_0 = 6.2$	0.12	0.64	0.96	0.96	0.64	0.12	0.573

$r_o = 3.5$ mm and $b_o = 6.2$ mm that results identical etching area. Cosine-tapering coefficients are determined by using (6).

Table 2: Tapering coefficients for square EBG structure and different n.

Tapering function	n	k_1	k_2	k_3	k_4	k_5	k_6	k_7	k_8	k_9	k_{10}	T_{cf}
Sine	3	0.71	1	0.71								0.807
Cosine		0.28	1	0.28								0.52
Sine	5	0.50	0.87	1	0.87	0.50						0.748
Cosine		0.16	0.76	1	0.76	0.16						0.568
Sine	10	0.28	0.54	0.76	0.91	0.99	0.99	0.91	0.76	0.54	0.28	0.696
Cosine		0.07	0.40	0.67	0.88	0.99	0.99	0.88	0.67	0.40	0.07	0.602
Binomial		0.01	0.07	0.29	0.67	1	1	0.67	0.29	0.07	0.01	0.408
Chebyshev		0.36	0.48	0.71	0.89	1	1	0.89	0.71	0.48	0.36	0.688

Cosine-tapering coefficients are determined by using (6).

T_{cf} among the considered functions. From the complete analysis of the different mentioned tapering methods, we have observed that the sine-tapered designs result in appreciable performance in all respects; hence, higher T_{cf} results in relatively wider stopband performance with higher insertion loss. Therefore, by T_{cf}, a preliminary prediction regarding the number of EBG elements and the required size of the reference EBG element is possible to obtain the desired performance. Furthermore, area tapering is the most appropriate type of tapering tactic for getting good bandwidth and IL performance since it offers a more distributed etching area under the transmission line.

6. Optimization of Sine-Tapered Design

Optimization of an EBG filter comprises two things: (a) deducing the optimized design (i.e., design optimization) and (b) performance optimization. Design optimization, basically, refers to the use of the optimal number of EBG structures and the optimal size of the reference EBG pattern.

6.1. Optimum Number of EBG Structures. First, to determine the most optimized design of the filter, we need to deduce the minimum required number of EBG elements to meet the desired goal regarding the space limitation (if any). In Table 5, we have presented the dependencies of the performance parameters on two variables: n and x_{ref}. For the square EBG pattern, during the first investigation (dependency with n), we considered the reference size of the square, b_{ref}, to be 6.2 mm. We have seen that as the number of EBG structures increases, the SBW, PBW, level of S_{21}, and RHs increase. As reported in [27], the minimum level of IL after the SBW remains lower as n increases. From the table, we can see that n can be suitably chosen in the range of 5 to 8, as they show better performance with a smaller size of the line.

6.2. Optimum Size of the Reference EBG Element. In the second investigation, the dependency of the performance on the size of the reference EBG element, we can observe that for a fixed $n = 7$, as the size of the reference element is increased, the SBW, the maximum level of S_{21} in the stopband, and the RHs get increased, and then band minimum S_{21} level remains lower. From Table 5, we can observe that the sizes of the reference square EBG pattern of 7.04 mm and 8.13 mm are −10.96 dB and −19.71 dB, respectively, whereas, for $b_{\text{ref}} = 4.7$ mm and 5.79 mm, the after-stopband levels of S_{21} are −2.25 dB and −5.31 dB, respectively, which is much more appreciable with much better SBWs and IL levels. Hence, the too-large size of the reference EBG element exhibits detrimental performance. Therefore, with $n = 7$, the optimum performance of the sine function (based on the area tapering method) can be obtained by choosing the size of the reference element between 4.7 mm and 5.79 mm. As the performance also depends on the number of EBG elements, for different n, the optimum size of the reference EBG structure should be readjusted.

6.3. Performance Optimization. In the above two optimizations, we have chosen the size of the EBG structure by calculating the filling factor, which is defined as (3), the ratio of the area of the reference EBG element to the area of a unit

Table 3: Performance of uniform and size-based tapered designs.

b_{ref} (mm)	n	Type of EBGS	−3 dB f_c (GHz)	−20 dB SBW (GHz)	f_0 (GHz)	S_{21} at f_0 (−dB)	Max. S_{21} (−dB)	−10 dB PBW (GHz)	Near SB RH (−dB)	Max. PB RH (−dB)
4.7	6	Uniform	7.609	4.07	10.458	37.31	37.45	7.56	2.92	2.92
		Binomial	7.504	—	—	—	12.54	5.96	0.68	0.68
		Chebyshev	7.582	—	—	—	19.03	7.19	0.14	0.36
		Cosine	7.603	—	—	—	14.92	7.15	0.13	0.31
		Sine	7.651	—	—	—	20.24	7.32	0.09	0.38
4.7	10	Uniform	7.774	4.67	10.398	51.75	51.76	7.43	3.35	3.35
		Binomial	7.735	—	—	—	16.58	6.69	1.21	0.31
		Chebyshev	7.81	2.915	10.476	32.22	32.48	7.59	0.11	0.44
		Cosine	7.804	2.634	10.504	28.52	28.70	7.62	0.13	0.43
		Sine	7.839	3.206	10.453	33.73	33.75	7.71	0.13	0.45
6.2	6	Uniform	7.036	5.885	10.416	48.98	50.57	6.15	5.19	5.19
		Binomial	6.906	—	—	—	20.44	5.68	1.21	0.87
		Chebyshev	7.037	3.751	10.562	31.72	31.73	6.72	0.13	0.73
		Cosine	7.013	2.484	10.498	25.64	25.56	6.66	0.14	0.62
		Sine	7.08	4.063	10.545	33.95	33.95	6.87	0.16	0.74
6.2	10	Uniform	6.854	6.099	10.428	48.31	51.48	6.76	3.60	3.6
		Binomial	6.928	3.28	10.476	26.97	27.40	6.40	0.15	0.70
		Chebyshev	7.2	4.917	10.419	46.37	60.44	7.00	0.07	0.84
		Cosine	7.238	5.057	10.435	42.89	50.47	7.10	0.13	0.83
		Sine	7.263	5.192	10.503	47.54	61.97	7.19	0.18	0.90

Cosine-tapering coefficients are determined by using (6).

cell, observing identical performance from the identical area of different EBG shapes [6]. Based on identical performance from different shapes, we have examined the impact of differing the number of EBG structures, n, in the area-based tapered designs while keeping the total etching area (A_{TE}) identical.

Table 6 shows that different sizes of reference EBG patterns are used in the designs for different n to maintain $A_{\text{TE}} = 168.14\,\text{mm}^2$. The size of the reference elements, x_{ref} (b_{ref} for square shape), is calculated by (5) and (11) as follows:

$$A_{\text{TE}} = \sum_{i=1}^{n} A_i. \tag{12}$$

From Table 6, we can notice that the maximum levels of S_{21} at the stopband are much lower with much higher values of minimum levels of S_{21} after the stopband for $n = 3$ and 4; furthermore, RHs are quite significant. On the other hand, as n increases, performance improvements are detected in terms of lower RH, the minimum level of S_{21} after stopband, and the maximum level of S_{21}; however, SBW reduces while passband width increases; and with a larger number of EBG structures, the total size of the design becomes longer. Therefore, keeping $n = 5$ to 8 in a sine-tapered design with a moderate A_{TE} (around $168\,\text{mm}^2$) will show optimum performance for the sine tapering method. With the area tapering method, engineers can achieve improved BW and IL performance. It eliminates the need to use a greater number of EBG elements and a very larger size of the reference EBG element; therefore, the whole design (i.e., length) becomes significantly smaller.

7. Tandem Designs and Performances

Tandem nonuniform EBG structures, basically, refer to the repeated use of the same set of nonuniform EBG patterns next to the one set, as shown in Figure 2.

7.1. Tandem Sine Tapering Function. Tandem design, in other words, means the use of the sine function for several half cycles of the angular distance since (4) represents that a set of coefficients is determined only by the angular distance of a sine wave for a half cycle. Tandem tapering coefficients, however, are determined by (4), where i is defined as a set of all discrete values in

$$i = 1, 2, 3, \cdots, \left[(n+1) \times C_r - 1\right], \tag{13}$$

where C_r is the number of repetitions of a set of tapered EBG structures (i.e., cycles) in the tandem design. The total number of EBG structures in a tandem design, N, is calculated by

$$N = C_r \times n. \tag{14}$$

Tandem coefficients might consist of several null points: values of i for which k_i becomes zero. For instance, if $C_r = 2$, then for $n = 5$, and we will have $N = 10$. Hence, the value of k_6 will become zero. There are three ways to treat the null point.

7.1.1. Type-1. Null locations will be kept in between the smallest EBG structures of two consecutive cycles of tapered EBG elements. The null location will have the spacing a, as in Figure 6(a).

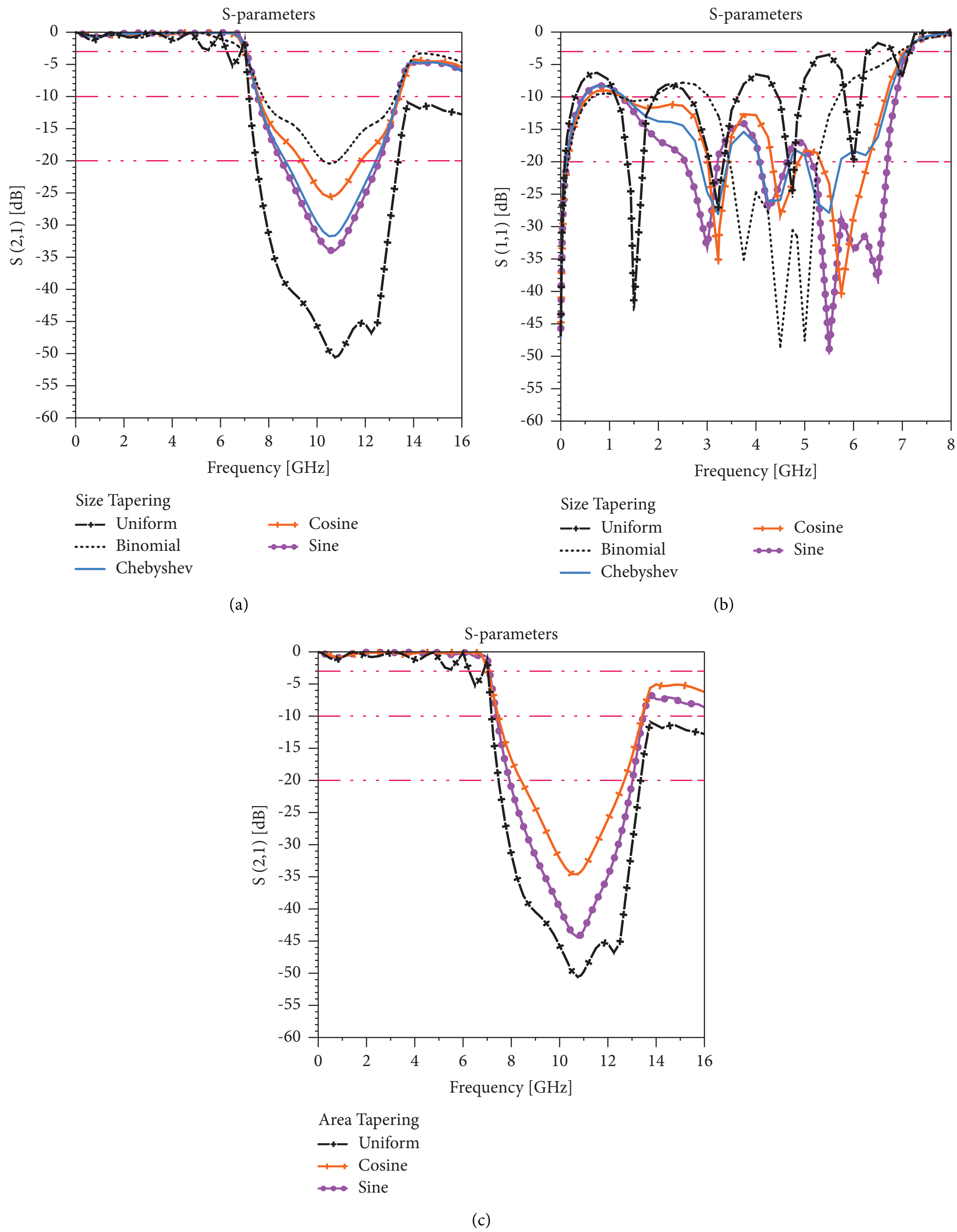

Figure 5: For different tapering functions, (a) insertion loss and (b) return loss of size-based tapered designs and (c) insertion loss of area-based tapered designs.

7.1.2. Type-2. Null points will be eliminated, and the next smallest EBG structures will be shifted to occupy the blank locations, as in Figure 6(b). Hence, the length of the transmission line becomes shorter than the Type-1 design, and it will be similar to the conventional tapered design with ten EBG elements.

7.1.3. Type-3. The two adjacent smallest EBG structures are merged as one, as shown in Figure 6(c); hence, N becomes 9 in this case. As a result, the length of the transmission line (L_t) is shortened by a when compared to the conventional tapered design with ten EBG elements and Type-2 designs

Table 4: Performance of different area-based tapered designs.

b_{ref} (mm)	n	Type of EBGS	−3 dB f_c (GHz)	−20 dB SBW (GHz)	f_0 (GHz)	S_{21} at f_0 -dB)	Max. S_{21} (−dB)	−10 dB PBW (GHz)	Near SB RH (−dB)	Max. PB RH (−dB)
4.7	6	Binomial	7.553	—	—	—	17.81	7.14	0.13	0.36
		Chebyshev	7.681	2.310	10.517	26.24	26.26	7.45	0.17	0.44
		Cosine	7.564	—	—	—	19.87	7.24	0.13	0.38
		Sine	7.701	2.515	10.510	27.12	27.13	7.49	0.32	0.47
4.7	10	Binomial	7.771	1.657	10.96	23.75	23.80	7.42	0.13	0.38
		Chebyshev	7.92	3.694	10.423	42.60	45.16	7.69	0.10	0.52
		Cosine	7.830	3.596	10.431	36.65	37.92	7.68	0.27	0.50
		Sine	7.872	3.824	10.415	42.89	45.64	7.75	0.14	0.53
6.2	6	Binomial	7.000	3.365	10.587	29.14	29.15	6.64	0.14	0.70
		Chebyshev	7.096	4.969	10.477	42.35	42.92	6.93	0.37	0.90
		Cosine	7.031	4.279	10.541	34.57	34.60	6.83	0.12	0.78
		Sine	7.097	5.094	10.473	43.51	44.40	6.88	0.72	0.92
6.2	10	Binomial	7.172	4.696	10.464	37.54	39.87	6.78	0.13	0.74
		Chebyshev	7.309	5.358	10.415	54.90	57.83	7.06	0.29	0.98
		Cosine	7.254	5.414	10.412	50.77	62.59	7.11	0.35	0.97
		Sine	7.288	5.482	10.414	51.10	56.10	7.19	0.16	1.00

Cosine-tapering coefficients are determined by using (6).

because L_t is usually assumed to be equal to Na. The total number of EBG elements in Type-3 designs will be

$$N_{\text{type}-3} = N - C_r + 1. \quad (15)$$

In Figure 6, we have depicted three types of tandem designs using circular EBG patterns, but we have realized the tandem designs with square EBG elements and considered area tapering using sine tapering coefficients, and the other designing specifications are identical to the earlier designs. Moreover, as of Table 6, we have considered $A_{\text{TE}} = 168.14\,\text{mm}^2$ for calculating the referent element for different n, C_r, and N. The size of the reference EBG element is calculated by

$$A_{\text{ref}} = \frac{A_{\text{TE}}}{C_r \sum_{i=1}^{n} k_i}. \quad (16)$$

Since the Type-3, tandem design has a lower number of EBG patterns; hence, the total etching area will be lower than the considered A_{TE}.

7.2. Performance of Different Tandem Designs. The performances of the tandem designs with $b_{\text{ref}} = 4.74$ mm are shown in Figure 7, where, unlike the conventional sine-tapered design, we can see two weird ripples in the S_{21} performance just before and after the stopband in the case of Type-1 and Type-2 designs for different values of n. Type-2 performs better than Type-1. Although they show undesired ripples near the stopband, the rest of the performance appears to be interesting when compared with the conventional sine-tapered designs that are presented in Table 6.

Besides, Type-3 exhibits better performance than the other two since it reduces the weird ripples significantly, as shown in Table 7. Since the Type-3 design possesses fewer EBG elements than the other tandem designs and their corresponding tapered designs, the total etching area is lower with a smaller transmission line. The transmission line becomes shorter by

$$\begin{aligned} T_{\text{sr}-t3} &= \left(1 - \frac{N_{\text{type}-3}}{N}\right) \times 100\% \\ &= \frac{C_r - 1}{N} \times 100\%. \end{aligned} \quad (17)$$

Thus, the numerical size of the transmission line is reduced by $(C_r - 1) \times a$.

Although using the Type-3 tandem design for relatively suitable values of n and C_r allows for smaller filters to be designed, a little malicious ripple near the stopband is the only factor preventing their use. We believe that the multiperiodicity issue is solely responsible for causing such abnormal ripples near the stopband [28].

7.3. Multiperiodicity in Tandem Designs. As we all know, electromagnetic bandgap structures should be placed at the bottom of transmission lines regularly because band rejection properties are solely dependent on the period [6, 18, 23]. The period, a, is

$$a = \frac{c}{2 f_0 \sqrt{\varepsilon_{\text{eff}}}}, \quad (18)$$

where ε_{eff} is the effective relative permittivity of the dielectric slab, c is the speed of light in free space, and f_0 is the center frequency of the stopband.

EBG structures, in tandem designs, experience multiperiodicity in two ways: (a) periodicity caused by the adjacent significant EBG elements of the smallest or edged elements of a cycle (primary cause) and (b) periodicity caused by the consecutive bigger elements from both sides of the smaller EBG structures (i.e., periodicity among the EBG elements of the same size in the nonuniform EBG array). Figure 8 illustrates the multiperiodicity clearly,

Table 5: Optimization of sine function-based design: "n" vs. size analysis.

n	b_{ref} (mm)	-3 dB f_c (GHz)	-20 dB SBW (GHz)	f_0 (GHz)	S_{21} at f_0 ($-$dB)	Max. S_{21} ($-$dB)	-10 dB PBW (GHz)	Near SB RH ($-$dB)	Max. PB RH ($-$dB)	After SB S_{21} ($-$dB)
4	6.2	6.921	3.618	10.649	28.51	28.53	6.71	0.35	0.71	5.51
5		7.032	4.775	10.519	36.55	36.74	6.89	0.50	0.83	6.42
6		7.097	5.094	10.473	43.51	44.40	6.88	0.72	0.92	6.63
7		7.16	5.29	10.447	52.14	46.97	7.13	0.38	0.97	6.93
8		7.236	5.366	10.435	65.03	67.93	7.19	0.16	1.02	7.49
9		7.282	5.515	10.419	49.49	60.79	7.13	0.38	1.04	8.09
7	4.07	8.183	1.592	10.486	23.52	23.50	7.89	0.19	0.35	1.13
	4.70	7.796	3.155	10.478	31.11	32.16	7.60	0.23	0.50	2.25
	5.79	7.316	4.869	10.457	46.68	47.11	7.18	0.31	0.82	5.31
	7.04	6.995	5.815	10.392	60.16	63.26	6.83	0.59	1.30	10.96
	8.13	6.825	6.096	10.299	53.44	53.52	6.88	1.56	1.80	19.71

Table 6: Optimization of sine tapering function with identical A_{TE}.

n	b_{ref} (mm)	-3 dB f_c (GHz)	-20 dB SBW (GHz)	f_0 (GHz)	S_{21} at f_0 ($-$dB)	Max. S_{21} ($-$dB)	-10 dB PBW (GHz)	Near SB RH ($-$dB)	Max. PB RH ($-$dB)	After SB S_{21} ($-$dB)
3	8.34	6.251	3.617	10.332	25.642	27.309	5.871	2.03	2.03	10.88
4	7.39	6.64	5.168	10.378	35.881	36.448	6.476	0.76	1.10	10.00
5	6.71	6.881	5.271	10.464	40.774	41.559	6.694	0.68	0.99	8.61
6	6.2	7.097	5.094	10.473	43.508	44.401	6.881	0.72	0.92	6.64
7	5.79	7.316	4.869	10.457	46.684	47.109	7.183	0.31	0.82	5.31
8	5.45	7.507	4.6	10.447	50.206	50.506	7.375	0.12	0.75	4.17
9	5.16	7.627	4.494	10.425	43.266	44.695	7.634	0.26	0.68	4.02
10	4.92	7.802	4.272	10.415	46.803	48.383	7.705	0.28	0.60	3.31
11	4.7	7.919	4.041	10.409	49.154	49.682	7.907	0.30	0.55	3.00
12	4.52	8.059	3.827	10.398	47.932	48.281	7.954	0.31	0.51	2.23

$A_{TE} = 168.14\,mm^2$.

where a is the original period; due to the much smaller EBG elements at the edge, the nearest bigger EBG elements offer a larger inner element spacing ($a' = 2a$), since smaller EBG elements have almost negligible effects on rejection property [24]. Moreover, the next bigger elements will offer different periods: $a'' = 4a$ and so on. Hence, the predominating larger period due to significantly bigger EBG elements causes such a high ripple that it seems another stopband is about to appear at another subsequent center frequency related to that period.

Since Type-3 tandem designs exhibit better performance than the other two types, therefore, we will consider only the Type-3 format as tandem use of tapered EBG elements, and by referring to tandem design, the Type-3 tandem fashion will be regarded. Now, with the objective of eliminating the unwanted near-band ripples, we have proposed the meandered line tandem (MLT) EBG filter with an even shorter physical size of the filter realization.

8. Proposed Meandered Line Tandem Design

In this section, we propose the method of meandered line tandem designs, where the smallest EBG structure between two consecutive cycles of tapered EBG elements is placed along the Y axis by bending the transmission line at a right angle on the top plane to go along all of the EBG elements at the ground plane. The length of the vertically bent part of the transmission line is always "a" for each smallest periodic element in the tandem design except the smallest elements at the corners; thus, the total minimum bending required is $C_r - 1$. However, bending for the corner element could also be incorporated as in Figure 13(c), but with no further advantage in size reduction. Therefore, the length will be shortened by $(C_r - 1) \times a$.

The tandem design of Figure 8 is converted as MLT design, as shown in Figure 9(a). The vertical length of the transmission line is a; thus, the horizontal length of the line becomes shorter by the length of a period, a. Therefore, the physical length of the filter realization becomes significantly shorter when compared to the conventional tapered design of the originally considered number of EBG elements. However, some differently bent transmission lines have been reported in [29, 30].

8.1. Realization of MLT Design. Let us first consider the same design illustrated in the conventional Type-3 tandem design ($n = 5$, $C_r = 2$; $b_{ref} = 4.74$ mm, $A_{TE} = 168.14\,mm^2$) in the earlier section, as shown in Figure 8, whose performance is shown in Figure 7: -6.30 dB and -6.94 dB ripples before and after the stopband, respectively. The MLT realization of this design is shown in Figure 9(a), where we can see that the smallest

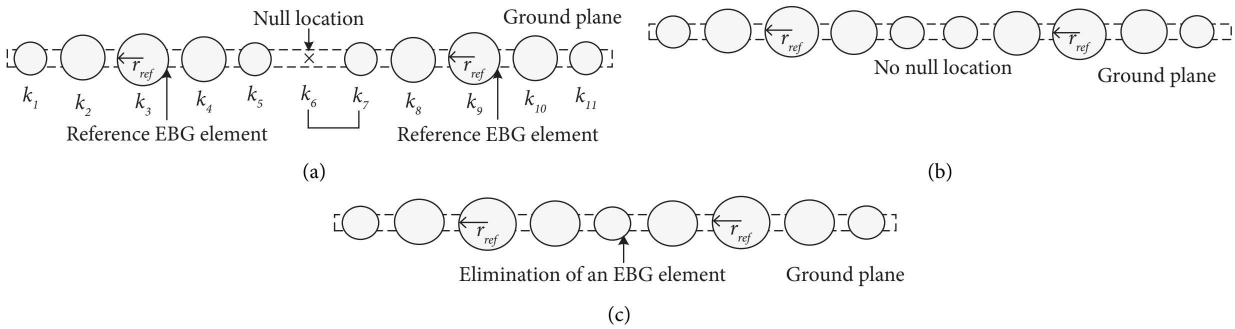

Figure 6: Tandem use of nonuniform EBG elements in the form of (a) Type-1: keeping null location, (b) Type-2: eliminating null location, and (c) Type-3: merging adjacent EBG structures of null location.

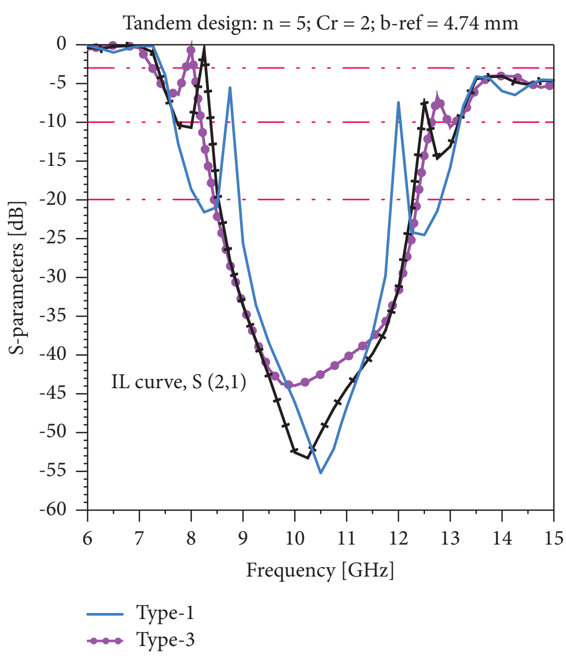

Figure 7: Insertion loss of different types sine function-based tandem designs.

element in between two consecutive cycles is placed vertically just beneath a deliberately bent transmission line, by which we have shortened the longitude of the transmission line by a.

Using (15), for conventional Type-3 tandem design, the required L_t is $9a$ for $n = 5$ and $C_r = 2$, and for $n = 3$ and $C_r = 3$, it is $7a$; hence, the size is reduced by 10% and 22.22%, respectively, compared to the uniform and conventional tapered design having $N = 10$, whereas in the case of MLT design, we have $L_t = 8a$ for $n = 5$ and $C_r = 2$ and $L_t = 5a$ for $n = 3$ and $C_r = 3$; thus, the size is reduced by 20% and 44.44%, compared to conventional tapered design and uniform design having $N = 10$ as well. Therefore, the MLT design and the Type-3 tandem design offer various scales of size reduction depending on the values of n and C_r shown in Table 7.

Furthermore, for the MLT design, the size is reduced by twice that of the Type-3 tandem design, $2a\ (C_r - 1)$. The length of the meandered transmission line is

$$L_{\mathrm{MLT}} = N_{\mathrm{MLT}} \times a, \tag{19}$$

where

$$N_{\mathrm{MLT}} = N - 2(Cr - 1). \tag{20}$$

Thus, the transmission line becomes shorter by

$$\begin{aligned} T_{\mathrm{sr-MLT}} &= \left(1 - \frac{L_{\mathrm{MLT}}}{\mathrm{Na}}\right) \times 100\% \\ &= 2T_{\mathrm{sr}-t3}. \end{aligned} \tag{21}$$

Note that, while designing the MLT design for $n = 3$, we deduced $b_{\mathrm{ref}} = 5.89\ \mathrm{mm}$ for $C_r = 2$ (i.e., $N = 5$) and $A_{\mathrm{TE}} = 168.14\ \mathrm{mm}^2$, but while we tried to design the MLT design as exactly similar to that shown in Figure 9(a), the two adjacent bigger EBG elements overlapped with the vertically placed EBG structure at the corners. Hence, designers should be careful about the limitation while deciding n and C_r.

However, such problems could be reduced in several ways: (a) we could reduce the size of the reference EBG elements to overcome the overlapping issue, (b) we could increase the cycle (C_r) of the tapered EBG elements, and (c) we could adopt the both to get optimum performance. Figure 9(b) shows a typical MLT design with $n = 3$ and $C_r = 3$ for a better understanding of the designing strategy with higher C_r, where we observed a 28.57% reduction in length for the nonmeandered line Type-3 design considered and the design is 44.44% shorter compared to the corresponding uniform and conventional tapered designs.

8.2. Performance of the MLT Design. The proposed MLT design exhibits quite impressive performance that significantly reduces the malicious ripples, as shown in Figure 10(a) with a reduced longitude of the design. Table 7 shows that the passband maximum RH is only −0.76 dB and the after-stopband ripple is eliminated; in addition, the SBW has increased to 4.523 GHz, which is very similar to the performance of the conventional area-based sine-tapered designs, shown in Figure 10(b); besides, the MLT design, in addition, offers a significant reduction in the filter size.

Table 7: Size reduction and performance of the MLT designs.

Type	b_{ref} (mm)	n	C_r	N	L_t	T_{sr} (%)	−3 dB f_c (GHz)	−20 dB SBW (GHz)	−10 dB PBW (GHz)	Max. PB RH (−dB)	After SB S_{21} (−dB)
Type-2	5.89	3	2	6	6a	0	7.349	4.953	7.404	5.30	7.40
Type-3				5	5a	16.7	7.176	4.714	7.173	2.85	6.40
Type-3	4.81	3	3	7	7a	22.2	8.09	3.134	7.987	2.16	2.66
MLT				5	5a	44.4	7.233	5.217	7.014	1.74	7.07
Type-2	5.22	4	2	8	8a	0	7.779	4.301	6.724	7.48	8.60
Type-3				7	7a	12.5	7.647	4.345	7.479	3.72	6.58
MLT				6	6a	25	6.917	5.408	6.676	0.84	7.03
Type-2	4.74	5	2	10	10a	0	8.282	3.749	8.390	10.60	7.50
Type-3				9	9a	10	8.05	3.922	8.068	6.30	6.94
MLT				8	8a	20	7.428	4.523	7.128	0.76	4.8
Type-2	4.39	6	2	12	12a	0	7.731	3.230	7.64	0.66	3.17
Type-3				11	11a	8.33	7.672	3.431	7.428	0.48	3.02
MLT				10	10a	16.7	7.699	3.908	7.494	0.68	2.95
Type-2	4.09	7	2	14	14a	0	7.966	2.835	7.904	0.49	2.37
Type-3				13	13a	7.14	7.89	2.974	7.816	0.67	2.63
MLT				12	12a	14.3	7.967	3.48	7.936	0.66	2.77

Sine tapering method is used and $A_{\text{TE}} = 168.14\,\text{mm}^2$. T_{sr} is the reduction of the length in percentage compared to corresponding uniform and conventional tapered designs.

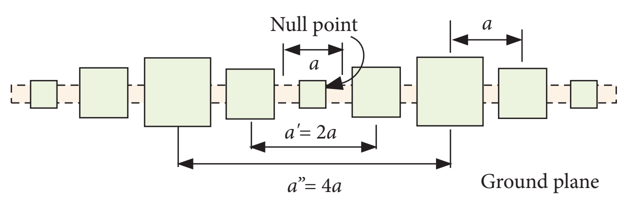

Figure 8: Illustration of multiperiodicity for Type-3 tandem design having $n = 5$ and $C_r = 2$; length of the transmission line is reduced by a compared to the conventional tapered design for $N = 10$, thus, $L_t = 9\ a$ in this design.

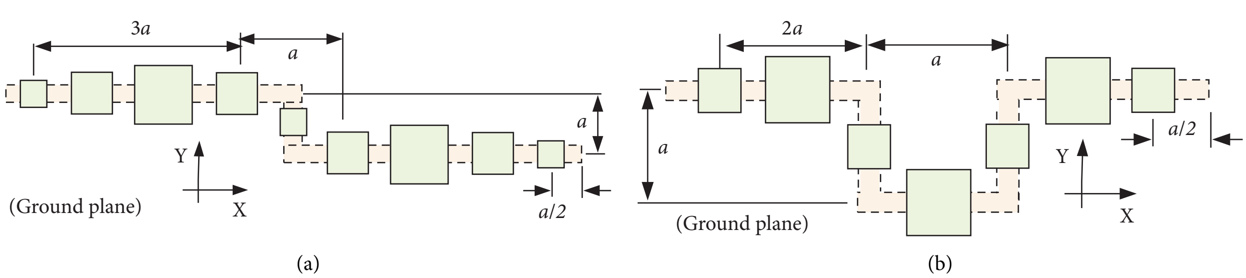

Figure 9: MLT designs based on area-based sine tapering function for (a) $n = 5$ and $C_r = 2$, and (b) $n = 3$ and $C_r = 3$. L_t for (a) and (b) are 8a and 5a, respectively; therefore, the lengths of the designs are reduced by 11.11% and 28.57%, respectively, than the corresponding tandem designs having $N = 9$.

The MLT design with $C_r = 3$ results in a larger stopband and maximum level of isolation compared to both Type-3 tandem designs for $C_r = 2$ and 3, shown in Figure 11 with smaller RHs. Tables 6 and 7 show that the SBW of the MLT realization for $n = 3$, $C_r = 3$, and $N = 7$ is 5.217 GHz, which is significantly higher than the SBWs of conventional tapered design: 4.869 GHz and 4.494 GHz for $n = 7$ and $n = 9$, respectively; however, a slight increase in the maximum RH is observed, which is happily acceptable with the benefit of huge size reduction and significant improvement in SBW.

Optimum performance can be achieved by choosing the proper size of the reference EBG element. In Figure 12, we observe that the smaller the reference EBG element, the lower the passband ripples, along with the lower maximum isolation level and smaller rejection bandwidth. Overall, it is clearly understood that the proposed MLT design based on the sine tapering function is very effective for relatively shorter filter realizations as long as area tapering and the Type-3 tandem strategy are considered.

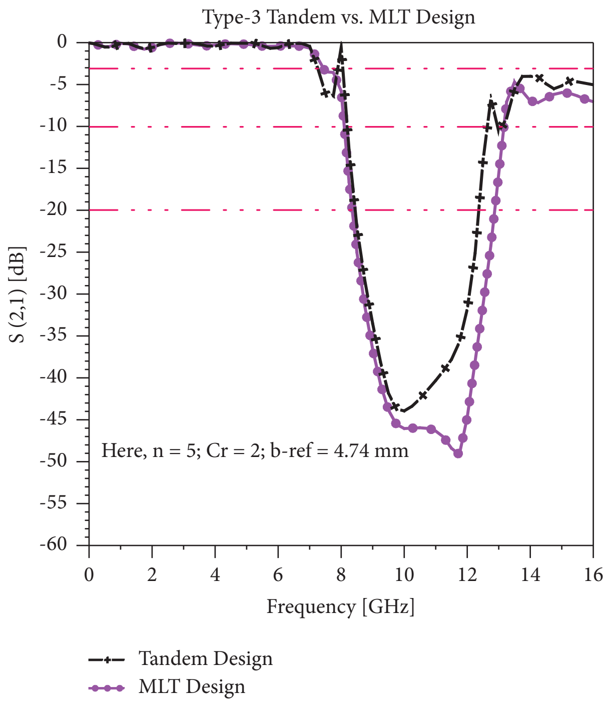

(a)

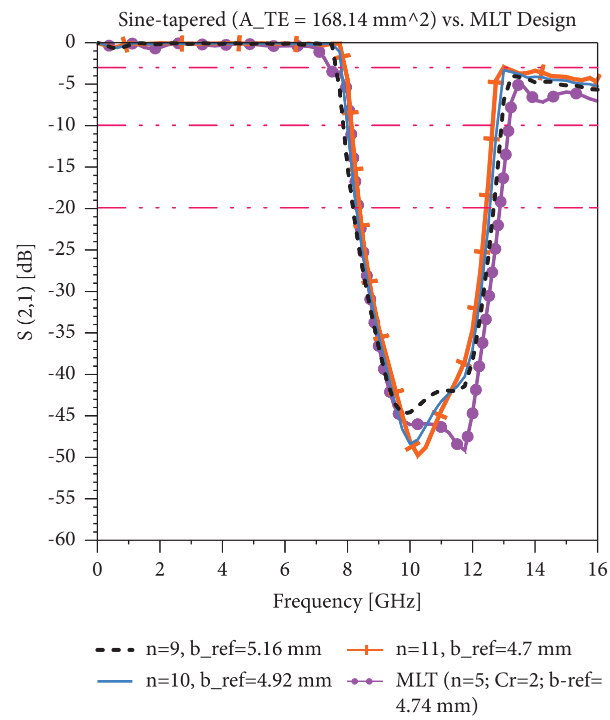

(b)

Figure 10: Performances of (a) Type-3 tandem vs. MLT designs with $n = 5$ and $C_r = 2$ and (b) conventional sine tapered vs. MLT design.

9. Simulated vs. Measured Performance

All the simulations, studied in this article, are simulated using the IE3D simulator, the software has found wide acceptance and gained popularity over the decades in the fields of EM designs and simulations as the simulated results well agree with the measured results [7, 22, 23, 25]. However, to investigate the validation of the simulated results in our case, we have considered the uniform circular EBG structure-assisted design illustrated in [31]. The design was simulated using HP™ momentum and ADS software and measured with HP™ 8753-D network analyzer.

Besides, the novel MLT approach for designing EBG filters improves the performance further with a much smaller filter realization. MLT design has potential applications in microstrip filters and microstrip array antenna designing with much smaller sizes in practice.

9.1. IE3D Simulation vs. Measured Performance. Since we currently lack the necessary experimental arrangement to measure the performances of our reported designs, hence, we have compared the simulated performance (obtained from IE3D software) of the same design with the measured and simulated performance reported by Chiau et al. in [31]. The designing parameters are $\varepsilon_r = 10.2$; $h = 1.27$ mils; $w = 1.2$ mm; and $a = 23.9$ mm for $f_o = 2.5$ GHz with $n = 9$ uniform circular EBG structures having the radius, $r = 5.975$ mm. The reported uniform design is shown in Figure 13(a).

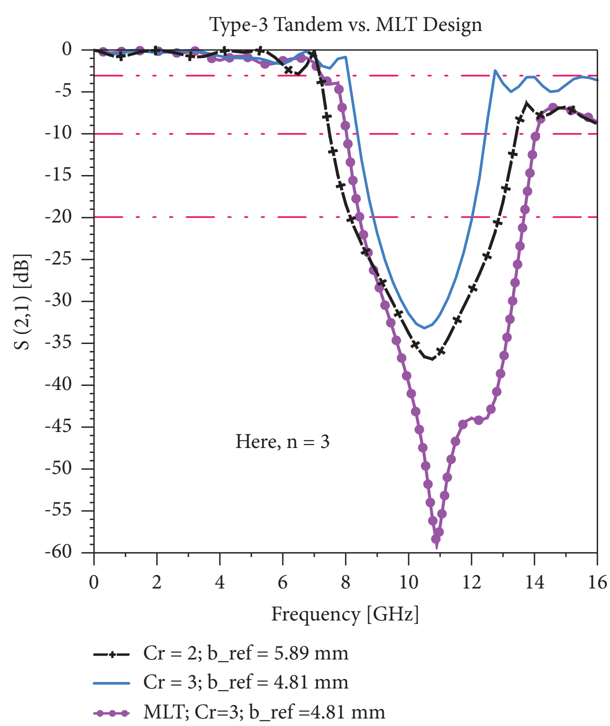

Figure 11: Performances of Type-3 tandem vs. MLT designs with $n = 3$ and $C_r = 3$.

The simulated performance using IE3D is compared with the reported measured result in Figure 14(a). We can see in the figure that the simulated result well agrees with the

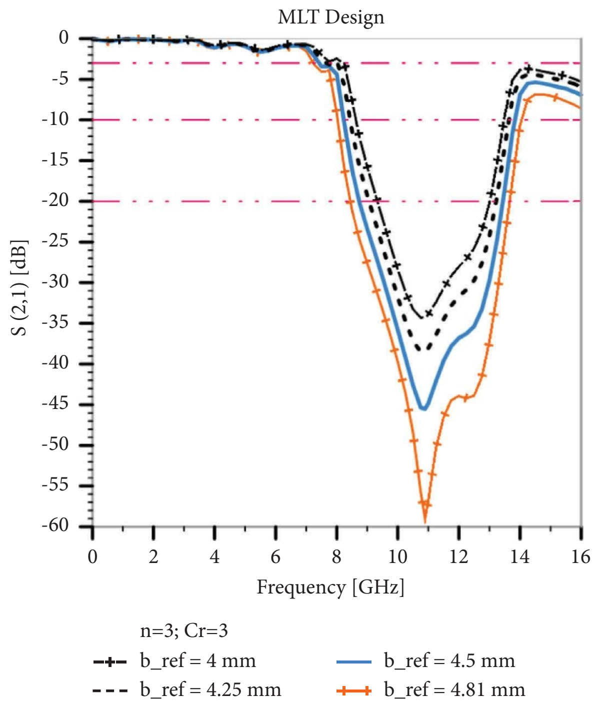

Figure 12: Optimizing the performance of MLT designs for $n = 3$ and $C_r = 3$ by varying the size of the reference EBG element.

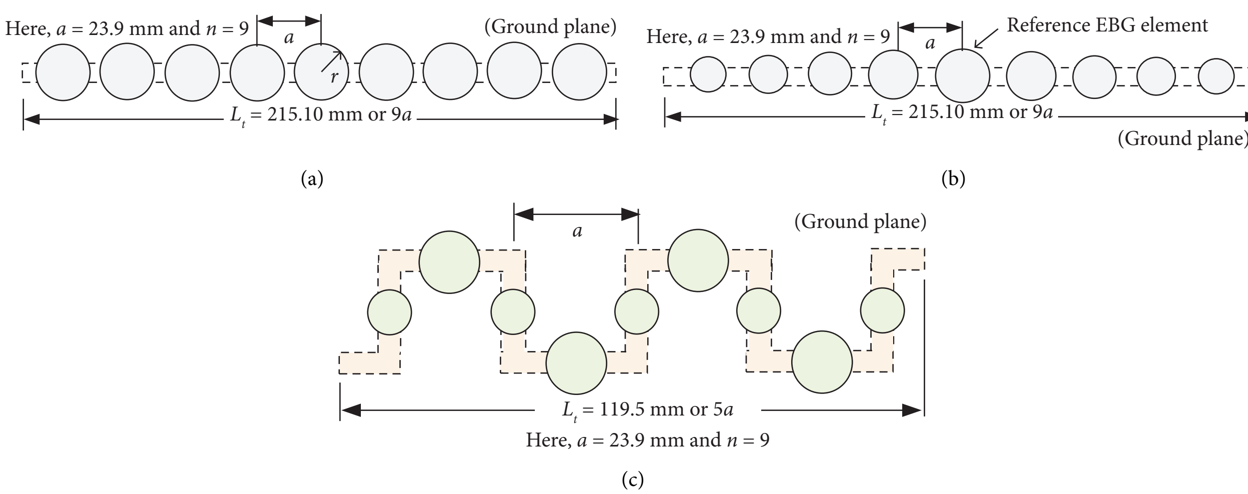

Figure 13: (a) Uniform circular EBG structure-assisted design reported in [31], corresponding (b) area-based sine-tapered design, and (c) MLT design with $C_r = 4$ and $n = 3$, where 44.44% length is reduced.

measured result that was obtained from HP™ 8753-D network analyzer. A little deviation is noticed that is generally well accepted by experts and researchers [18, 23, 25]. Moreover, in Figures 3 and 4, we have noticed such good agreement between the simulated results (using the IE3D software) and the measured results of different designs reported in [18, 25].

9.2. IE3D Simulation vs. ADS Simulation. In Figure 14(b), we observe that the simulated result of the earlier described uniform design using IE3D identically agrees with the reported simulated performance using ADS software that is presented in [31].

Moreover, from the comparison of Figures 14(a) and 14(b), we can notice that the similar deviation between simulated and measured results is accepted by the authors too in [31].

9.3. Performance Validation of the Latest Designs. As from the abovementioned discussions, we have observed very well agreement of our simulated results with measured results and simulated results using other software; therefore, we have applied the proposed sine tapering method (Figure 13(b)) of improving the performance and the meandered line tandem design (Figure 13(c)) approach to reduce the size of the whole design to the earlier illustrated design and compared the

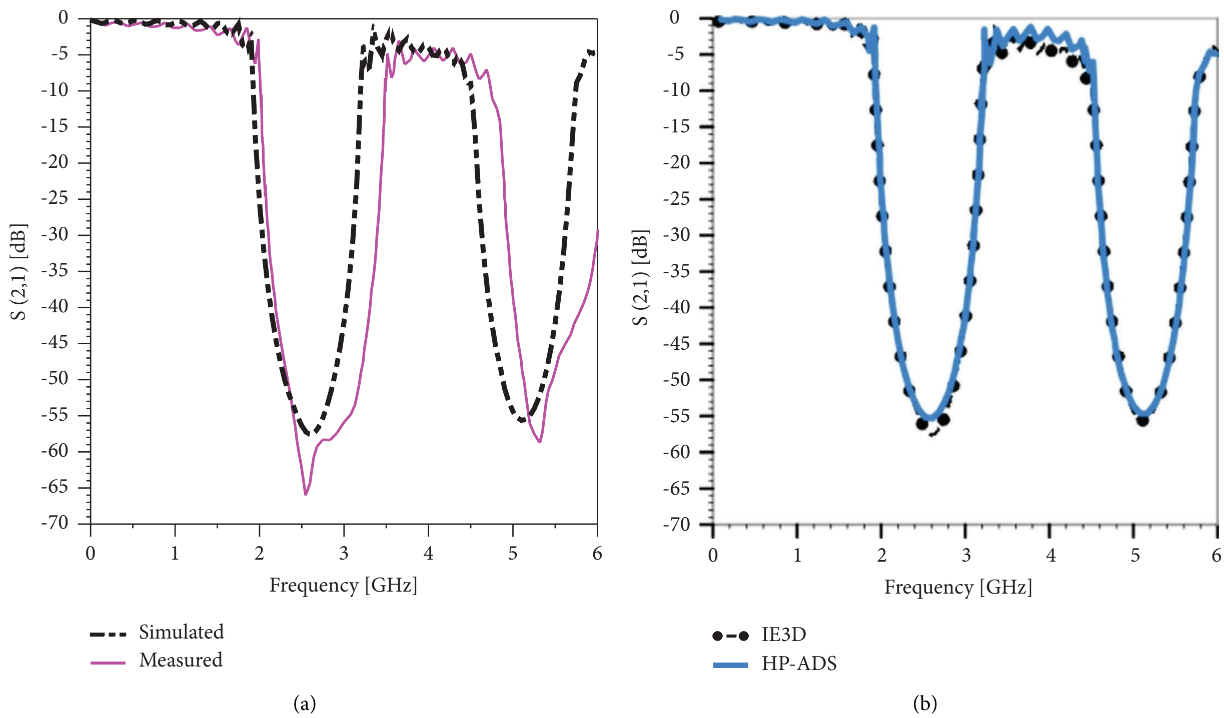

Figure 14: S-parameter performance of uniform circular EBG structure-assisted design reported in [31]: (a) simulated using IE3D software vs. measured and (b) simulated using IE3D software vs. ADS software. Insertion loss performance for, r = 5.975 mm, n = 9, a = 23.9 mm.

Table 8: Uniform design vs. sign tapered and meandered line tandem design.

Type	No. of EBG element (N)	Length (L_t)	% size reduction (T_{sr})	−3 dB f_c (GHz)	−20 dB SBW (GHz)	−10 dB PBW (GHz)	Max. PB RH (−dB)
Uniform*	9	$9a$	0	1.90	1.19	1.77	4.01
Sine tapered#	9	$9a$	0	1.91	0.98	1.88	0.84
Identical area sine tapered**	9	$9a$	0	1.86	1.26	1.87	1.28
MLT	9	$5a$	44.44	1.81	1.22	1.77	2.14

*A_{TE} = 1009.414 mm^2. #Area-based sine tapering method is used. **Total etching area is identical to the uniform design.

simulated performances with the performance of the conventional uniform design (Figure 13(a)).

In Figure 13, we notice that the MLT design consists of $C_r = 4$ with $n = 3$; thus, the size of the physical design becomes 44.44% shorter compared to the corresponding uniform design and corresponding sine-tapered design as well as any other tapered design, as shown in Table 8.

In Figure 15, we see the performance of the MLT design is quite matched with the performance of the corresponding uniform design. Besides, the performance patterns of sine-tapered designs are similar to the performance pattern of the uniform design with expected behavior. Therefore, we are confident that our studies' simulated results agree with the measured results.

However, in Table 8, we observe that the performance of the MLT design results in a wider stopband width and smaller passband ripples compared to the uniform design. On the other hand, identical area sine-tapered design exhibits a wider stopband with much smaller passband ripples. However, the proposed MLT designing strategy will certainly benefit the designers where limited space is a concerning issue, e.g., in satellites and space communication applications.

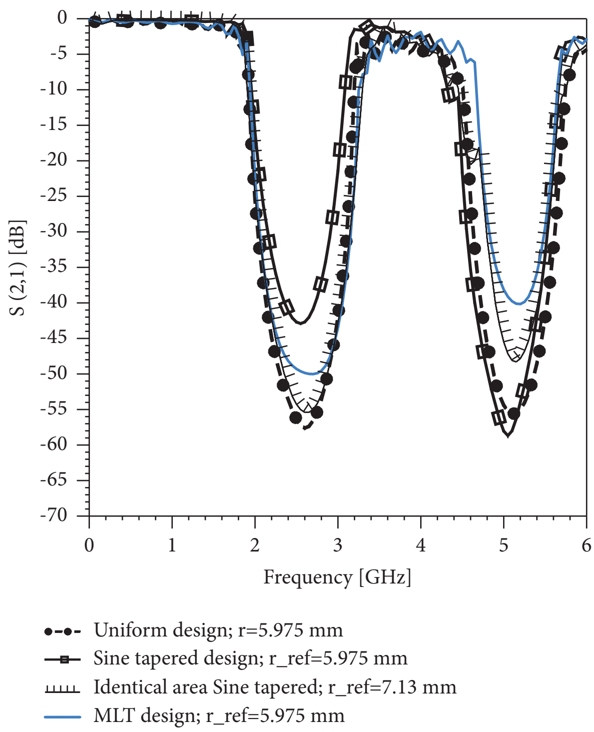

Figure 15: Simulated results (using the IE3D software) of uniform circular EBG element-assisted design reported in [31] vs. area-based sine-tapered design and MLT design.

10. Conclusion

The discussed simpler technique of tapering EBG patterns using the sine function results in outstanding performance compared to the other widely used tapering methods. It shows better IL property, a wider stopband, and smaller ripples in the performance. The area tapering method, in particular, outperforms the uniform and size tapering designs in terms of performance. Furthermore, we have observed the optimized performance of the sine-tapered design for the total etching area of 168.14 mm^2 with 5 to 8 EBG structures, taking area tapering into account.

Besides, the novel MLT approach for designing EBG filters improves the performance further with a much smaller filter realization, approximately 15% to 45% depending on the choice of designing parameters. MLT design has potential applications in designing microstrip filters and microstrip array antennas for microwave communication systems to fulfill the requirement of smaller size realization.

Data Availability

The data used to support the findings of this study are made available from the corresponding author upon request.

Conflicts of Interest

The authors declare that they have no conflicts of interest.

Acknowledgments

This research work was partially funded by the Center for Research and Development (CRD), Eastern University, Road 6, Block B, Ashulia Model Town, Savar, Dhaka, Bangladesh (https://www.easternuni.edu.bd/CRD).

References

[1] P. Dalal and S. K. Dhull, "Electromagnetic band gap structure applications in modern wireless perspective: a review," in *Proceedings of the 2019 International Conference on Advances in Computing and Communication Engineering (ICACCE)*, pp. 1–6, IEEE, Sathyamangalam, India, April 2019.

[2] P. Zuo, Y. Li, E. P. Li, T. Song, M. Wang, and H. Zheng, "A novel electromagnetic bandgap design applied for suppression of printed circuit board electromagnetic radiation," *International Journal of RF and Microwave Computer-Aided Engineering*, vol. 30, no. 1, Article ID e21990, 2020.

[3] A. M. Hediya, A. M. Attiya, and W. S. El-Deeb, "5G MIMO antenna system based on patched folded antenna with EBG substrate," *Progress in Electromagnetics Research M*, vol. 109, pp. 149–161, 2022.

[4] M. Pant and L. Malviya, "Design, developments, and applications of 5G antennas: a review," *International Journal of Microwave and Wireless Technologies*, vol. 15, pp. 156–182, 2022.

[5] L. Inclán-Sánchez, "Inverted microstrip gap waveguide coplanar EBG filter for antenna applications," *Electronics*, vol. 11, no. 18, p. 2951, 2022.

[6] S. S. Hassan and M. N. Mollah, "Identical performance from distinct conventional electromagnetic bandgap structures," *IET Microwaves, Antennas & Propagation*, vol. 10, no. 12, pp. 1251–1258, 2016.

[7] N. C. Karmakar and M. N. Mollah, "Investigations into nonuniform photonic-bandgap microstripline low-pass filters," *IEEE Transactions on Microwave Theory and Techniques*, vol. 51, no. 2, pp. 564–572, 2003.

[8] S. Patil, A. Verma, A. Kumar Singh, B. K. Kanaujia, and S. Kumar, "A low-profile circularly polarized microstrip antenna using elliptical electromagnetic band gap structure," *International Journal of Microwave and Wireless Technologies*, vol. 14, no. 8, pp. 1–10, 2021.

[9] E. G. Ouf and A. S. Abd El-Hameed, "Design of low pass filter with ultra-wide stopband based on DGS and SIRs," *AEU-International Journal of Electronics and Communications*, vol. 137, Article ID 153795, 2021.

[10] S. Modak and T. Khan, "Cuboidal quad-port UWB-MIMO antenna with WLAN rejection using spiral EBG structures," *International Journal of Microwave and Wireless Technologies*, vol. 14, no. 5, pp. 626–633, 2022.

[11] H. R. Zhu, Y. F. Sun, and X. L. Wu, "A compact tapered EBG structure with sharp selectivity and wide stopband by using CSRR," *IEEE Microwave and Wireless Components Letters*, vol. 28, no. 9, pp. 771–773, 2018.

[12] N. Melouki, A. Hocini, and T. A. Denidni, "Performance enhancement of a compact patch antenna using an optimized EBG structure," *Chinese Journal of Physics*, vol. 69, pp. 219–229, 2021.

[13] D. Karatzidis, A. Apostolidis, S. Amanatiadis, and N. Kantartzis, "Genetically-optimized electromagnetic bandgap structures for efficient 5G implementations," in *Proceedings of the 2022 11th International Conference on*

Modern Circuits and Systems Technologies (MOCAST), pp. 1–4, IEEE, Bremen, Germany, June 2022.

[14] M. Bozzetti, A. D'Orazio, M. De Sario, V. Petruzzelli, F. Prudenzano, and F. Renna, "Tapered photonic bandgap microstrip lowpass filters: design and realisation," *IEE Proceedings Microwaves, Antennas and Propagation*, vol. 150, no. 6, pp. 459–462, 2003.

[15] C. Maximo-Guti´errez, J. Hinojosa, F. L. Martínez-Viviente, and A. Alvarez-Melcon, "Design of high-performance microstrip and coplanar low-pass filters based on electromagnetic bandgap (EBG) structures," *AEU-Int J. Electron Commun.*, vol. 123, 2020.

[16] Y. Kawaguchi, K. Saitoh, and M. Koshiba, "Design of taper structure for highly efficient coupling between 1-D photonic crystal coupled resonator optical waveguide and straight waveguide," *Journal of Lightwave Technology*, vol. 27, no. 14, pp. 2924–2929, 2009.

[17] J. D. D. Ruiz, F. L. Martínez-Viviente, and J. Hinojosa, "Optimisation of chirped and tapered microstrip Koch fractal electromagnetic bandgap structures for improved low-pass filter design," *IET Microwaves, Antennas & Propagation*, vol. 9, no. 9, pp. 889–897, 2015.

[18] M. A. G. Laso, M. J. Erro, T. Lopetegi, D. Benito, M. J. Garde, and M. Sorolla, "Optimization of tapered Bragg reflectors in microstrip technology," *International Journal of Infrared and Millimeter Waves*, vol. 21, no. 2, pp. 231–245, 2000.

[19] A. D'Orazio, M. De Sario, V. Gadaleta, V. Petruzzelli, and F. Prudenzano, "Meander microstrip photonic bandgap filter using a Kaiser tapering window," *Electronics Letters*, vol. 37, no. 19, pp. 1165–1167, 2001.

[20] E. Sandi, F. Y. Zulkifli, and E. T. Rahardjo, "A hybrid technique using combinatorial cyclic difference sets and binomial amplitude tapering for linear sparse array antenna design," *Advanced Electromagnetics*, vol. 5, no. 3, pp. 73–79, 2016.

[21] C. A. Balanis, *Antenna Theory: Analysis and Design*, John Wiley & Sons, Hoboken, NJ, USA, 2015.

[22] N. C. Karmakar, "Improved performance of photonic bandgap microstripline structures with the use of Chebyshev distributions," *Microwave and Optical Technology Letters*, vol. 33, no. 1, pp. 1–5, 2002.

[23] S. Y. Huang and Y. H. Lee, "Tapered dual-plane compact electromagnetic bandgap microstrip filter structures," *IEEE Transactions on Microwave Theory and Techniques*, vol. 53, no. 9, pp. 2656–2664, 2005.

[24] S. M. S. Hassan and M. N. Mollah, "Offset EBGS against tapered EBGS: substantial reduction of microstrip stopband filter in size," in *Proceedings of the 2016 IEEE Region 10 Conference (TENCON)*, pp. 3859–3862, IEEE, Singapore, November 2016.

[25] N. C. Karmaker and M. N. Mollah, "Potential applications of PBG engineered structures in microwave engineering: Part I," *Microwave Journal*, vol. 47, no. 7, pp. 22–44, 2004.

[26] S. M. S. Hassan, M. N. Mollah, S. M. Anayetullah et al., "Realization of low-pass filters from arbitrarily designed nonuniform EBG structures," in *Proceedings of the 2013 International Conference on Electrical Information and Communication Technology (EICT)*, pp. 1–6, IEEE, Khulna, Bangladesh, February 2014.

[27] M. N. Mollah and N. C. Karmakar, "Effect of number of uniform photonic bandgap (UPBG) elements on the performance of microstrip transmission lines," in *Proceedings of the 2003 IEEE Pacific Rim Conference on Communications Computers and Signal Processing (PACRIM 2003)*, pp. 62–65, Victoria, Canada, August 2003.

[28] C. C. Chiau, X. Chen, and C. Parini, "Multiperiod EBG structure for wide stopband circuits," *IEE Proceedings-Microwaves, Antennas and Propagation*, vol. 150, no. 6, pp. 489–492, 2003.

[29] S. C. Bera, R. V. Singh, V. K. Garg, N. S. Arora, and S. S. Nair, "A novel PBG structure for filter application," *Microwave and Optical Technology Letters*, vol. 48, no. 1, pp. 188–190, 2006.

[30] R. T. Hammed and Z. M. Abdul-Jabbar, "Multilayered stepped impedance loaded-resonator for compact dual-band rejection filter design," *Electromagnetics*, vol. 37, no. 8, pp. 493–499, 2017.

[31] T. Lopetegi, M. A. G. Laso, M. J. Erro et al., "Novel photonic bandgap microstrip structures using network topology," *Microwave and Optical Technology Letters*, vol. 25, no. 1, pp. 33–36, 2000.